Received: 28 September 2022 | Accepted: 15 November 2022

DOI: 10.1002/pamm.202200039

Phase-field modeling of crack propagation based on multi-crack order parameters considering mechanical jump conditions

Lukas Schöller[1,2,*], **Daniel Schneider**[1,2], **Andreas Prahs**[1], and **Britta Nestler**[1,2]

[1] Institute for Applied Materials (IAM-MMS), Karlsruhe Institute of Technology (KIT), Strasse am Forum 7, 76131 Karlsruhe, Germany

[2] Institute of Digital Materials Science (IDM), Karlsruhe University of Applied Sciences, Moltkestrasse 30, 76133 Karlsruhe, Germany

The phase field method is commonly used for the crack propagation modeling in modern material science, as they allow for an implicit tracking of the crack surface. However, most of these crack propagation models are for homogeneous materials, and there exist only a few approaches for heterogeneous systems. Recently, Schöller et al. [1] presented a novel phase-field model for multiphase materials, e.g. composites, based on multi-crack crack order parameters. Despite the quantitative advantages of the model, it is based on a simple scheme for the underlying homogenization problem. In this work, a more advanced homogenization scheme based on mechanical jump condition is applied to the model. Consideration of these jump conditions yields phase-specific stresses and strains. Therefore, the mechanical driving force for crack propagation can be modeled as more independent of the elastic properties of other physical regions. Volume elements of a fiber reinforced polymer are used to demonstrate the limitations of the simple scheme, as well the improvement if considering mechanical jump conditions. Thereby, the contrast in the crack resistance of the two materials is varied. It is shown that the simple linear interpolation does not lead to reasonable crack paths for contrary contrasts of elastic modulus and crack resistance. Taking into account the mechanical jump conditions instead yields still reasonable results. For both the final crack paths and the stress-strain curves of the system, the novel model is less sensitive to a change in fiber crack resistance. While the result of the simple scheme depend on the selected fiber crack resistance, although failure of the matrix is expected.

1 Introduction

Modern high-performance materials such as fiber-reinforced polymers (FRP) often offer high specific material properties, e.g. stiffness or fracture toughness. Due to their complex morphology, their material behavior is heterogeneous. Therefore, the prediction of crack propagation paths in such materials is of great interest as it improves the ability to determine effective load capacity and develop efficient, safe, and predictable products. Despite various approaches are discussed in literature, understanding the failure and fracture behavior of heterogeneous materials is still a major challenge in modern engineering. Although it has been demonstrated that linear elastic fracture mechanics (LEFM) may accurately describe crack propagation in homogeneous materials in two dimensions [2], a generalized method for modeling complex heterogeneous materials appears to be challenging and unfeasible. Cohesive zone modeling (CZM), developed by Barenblatt [3] and Dugdale [4], is an alternative approach that can be incorporated with the finite element method (FEM). More complex fracture paths necessitate complicated remeshing techniques, since these models demand conforming meshes. In contrast, the generalized finite element method (GFEM) extends the FEM solution space to handle discontinuous functions [5]. Nevertheless, both CZM and XFEM are limited in their ability to describe fracture mechanisms, such as crack nucleation or crack branching. The phase-field method (PFM), which introduces order parameters to enable a smooth transition between subregions, is a different way for handling singular interfaces. This yields continuous order parameters, often described as phase fields, and allows implicit tracking of the surface boundary on nonconforming meshes. Therefore, the PFM is widely established to describe the evolution of microstructures, and various phase-field approaches to brittle fracture have been developed, cf. e.g., [6–8]. A varying crack surface energy is incorporated into the majority of phase field models that describe fracture propagation in heterogeneous systems. This is accomplished either through an anisotropic surface energy, e.g. [9], or an interpolation of the surface energy, e.g. [10–12]. However, as recently discussed by Henry [13] and Schöller et al. [1], these approaches have some limitations as they can lead to nonphysical fracture behavior. Schöller et al. [1] presented an alternative approach for a phase-field crack propagation model in heterogeneous materials by introducing multi-crack order parameters (MCOP). This resulted in an improvement of the ability to describe crack propagation in such complex systems. The objective of the work at hand is to extend this model by incorporating a more sophisticated scheme for the underlying homogenization problem [14–19]. Therefore, the work of Schneider et al. [18] is applied to the MCOP model. Finally, an exemplary FRP system is used to demonstrate the limitations of the basic scheme and the advantages of the proposed model, where the homogenization scheme is based on mechanical jump conditions.

* Corresponding author: e-mail lukas.schoeller@kit.edu

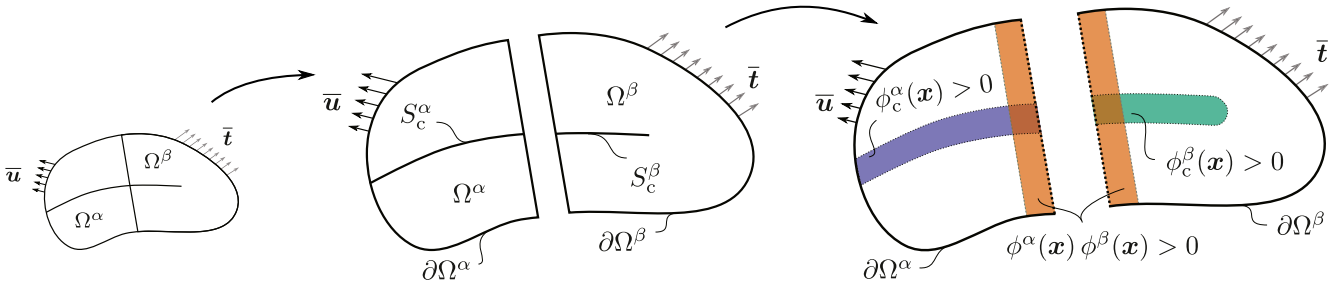

Fig. 1: Schematic heterogeneous body: The initial body is schematically shown on the left. In the center, the subregions are shown separately, with sharp crack interfaces. In the right figure, the model is shown with its diffuse crack interfaces in subregions Ω^α and Ω^β. The diffuse solid interface is highlighted in orange. Adapted from [1].

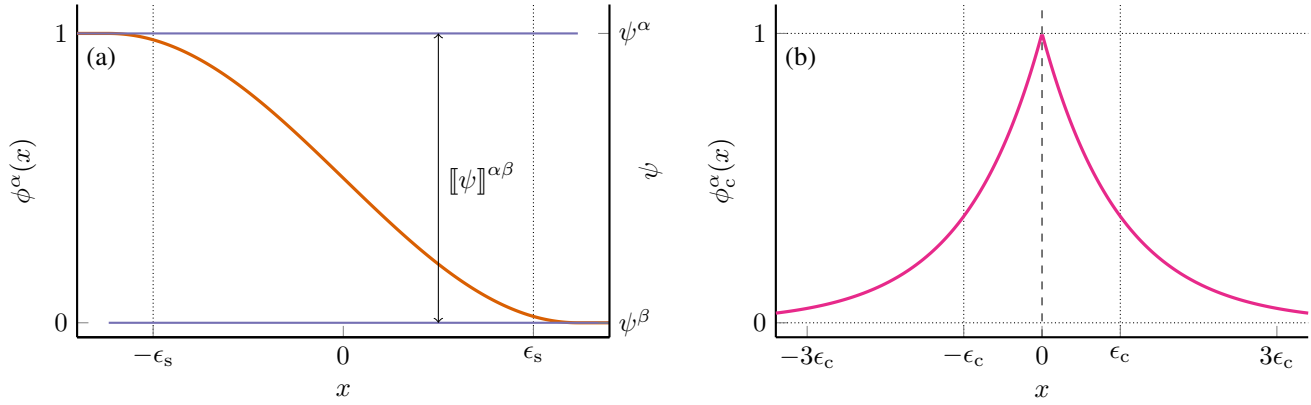

Fig. 2: Analytical order parameter profile for a solid interface (a) and a crack interface (b), for a corresponding sharp interface at $x = 0$. In addition, a jump $[\![\psi]\!]^{\alpha\beta}$ of an exemplary field ψ is illustrated.

2 Multi crack order parameter phase-field model

For a material body Ω consisting of N subregions Ω^α with varying physical properties, e.g. different phases or grains, and sharp crack surfaces S_c^α, cf. Figure 1, the free energy can be described by

$$\mathcal{F}[\boldsymbol{u}] = \sum_\alpha^N \int_{\Omega^\alpha} f_\mathrm{el}^\alpha(\boldsymbol{u})\,\mathrm{d}v + \sum_\alpha^N \int_{S_\mathrm{c}^\alpha} G_\mathrm{c}^\alpha\,\mathrm{d}a. \tag{1}$$

With a phase-specific strain energy density f_el^α and a critical energy release rate G_c^α. Based on e.g. the work of Nestler et al. [20] this material body can also be parametrized by a tuple of order parameters

$$\boldsymbol{\phi} = \left\{\phi^1, \phi^2, \ldots, \phi^N\right\}, \text{ with } \sum_{\alpha=1}^N \phi^\alpha = 1. \tag{2}$$

As each order parameter $\phi^\alpha \in [0,1]$ represents the local volume fraction of the corresponding subregion, the latter constraint has to hold. In this work, these order parameters are used to provide a diffuse interface between different subregions, cf. Figure 2a. In addition, a second tuple of crack order parameters

$$\boldsymbol{\phi}_\mathrm{c} = \left\{\phi_\mathrm{c}^1, \phi_\mathrm{c}^2, \ldots, \phi_\mathrm{c}^N\right\}, \tag{3}$$

is introduced to track the local damage to a material point in respect to the volume of the corresponding subregion [1, 21] and therefore representing the sharp crack surfaces S_c^α. Based on these sets of order parameters, the free energy of a heterogeneous body is approximated by the functional

$$\mathcal{F}[\boldsymbol{u}, \boldsymbol{\phi}, \boldsymbol{\phi}_\mathrm{c}, \nabla\boldsymbol{\phi}_\mathrm{c}] = \int_\Omega \left(\sum_\alpha^N \phi^\alpha h(\phi_\mathrm{c}^\alpha)\, f_\mathrm{el}^\alpha + \frac{1}{2}\phi^\alpha G_\mathrm{c}^\alpha \left(\epsilon_\mathrm{c} \left|\nabla\phi_\mathrm{c}^\alpha\right|^2 + \frac{1}{\epsilon_\mathrm{c}} \left(\phi_\mathrm{c}^\alpha\right)^2 \right) \right) \mathrm{d}v, \tag{4}$$

with a degradation function $h(\phi_\mathrm{c}^\alpha)$. The resulting diffuse interface from broken ($\phi_\mathrm{c}^\alpha = 1$) to unbroken material ($\phi_\mathrm{c}^\alpha = 0$) is characterized by the length scale parameter ϵ_c, cf. Figure 2b. In addition, the free energy of a subregion Ω^α follows by [1]

$$\mathcal{F}^\alpha[\boldsymbol{u}, \phi_\mathrm{c}^\alpha, \nabla\phi_\mathrm{c}^\alpha] = \int_{\Omega^\alpha} h(\phi_\mathrm{c}^\alpha)\, f_\mathrm{el}^\alpha + \frac{1}{2} G_\mathrm{c}^\alpha \left(\epsilon_\mathrm{c} \left|\nabla\phi_\mathrm{c}^\alpha\right|^2 + \frac{1}{\epsilon_\mathrm{c}} \left(\phi_\mathrm{c}^\alpha\right)^2 \right) \mathrm{d}v. \tag{5}$$

In contrast to the energy of the whole body there is no interpolation in terms of the order parameters ϕ^α present, which leads to a constant crack surface energy density. Following the approach of Kuhn and Müller [22] and Schneider et al. [18] the minimization of the free energy $\mathcal{F}$ results in the balance of linear momentum

$$\nabla \cdot \left(\sum_{\alpha}^{N} \phi^\alpha h(\phi_\mathrm{c}^\alpha)\, \boldsymbol{\sigma}^\alpha \right) = \mathbf{0}, \tag{6}$$

with the phase-specific stress tensors $\boldsymbol{\sigma}^\alpha$, regarding quasi-static behavior and vanishing body forces. The evolution equations of the crack order parameters are postulated as Allen-Cahn-type equations based on the minimization of $\mathcal{F}^\alpha$, reading

$$\dot{\phi}_\mathrm{c}^\alpha \frac{1}{M^\alpha} = G_\mathrm{c}^\alpha \left(\Delta\phi_\mathrm{c}^\alpha - \frac{1}{\epsilon_\mathrm{c}^2}\phi_\mathrm{c}^\alpha \right) - \frac{1}{\epsilon_\mathrm{c}} \frac{\partial h(\phi_\mathrm{c}^\alpha)}{\partial \phi_\mathrm{c}^\alpha} f_\mathrm{el}^\alpha, \quad \forall \alpha = 1, \dots, N. \tag{7}$$

A more detailed introduction of the MCOP model, presented in the work at hand, is given by Schöller et al. [1].

3 Mechanical jump conditions

The phase-specific strain energy densities f_el^α are modeled by hyperelastic potentials. Assuming small deformations

$$f_\mathrm{el}^\alpha = \frac{1}{2}\boldsymbol{\sigma}^\alpha \cdot \boldsymbol{\varepsilon}^\alpha, \qquad \boldsymbol{\sigma}^\alpha = \mathbb{C}^\alpha \left[\boldsymbol{\varepsilon}^\alpha\right], \tag{8}$$

follows, with the phase-specific infinitesimal strain tensor $\boldsymbol{\varepsilon}^\alpha$ and the stiffness tensor $\mathbb{C}^\alpha$. In general, the relation between phase-specific strains and the total strain tensor

$$\boldsymbol{\varepsilon} = \sum_{\alpha} \phi^\alpha \boldsymbol{\varepsilon}^\alpha = \mathrm{sym}\left(\mathrm{grad}\left(\boldsymbol{u}\right)\right), \tag{9}$$

with the displacement vector $\boldsymbol{u}$, is unknown. Schöller et al. [1] used a Voigt-Taylor homogenization scheme, for which $\boldsymbol{\varepsilon}^\alpha = \boldsymbol{\varepsilon}\ \forall \alpha = 1, \dots, N$ is assumed. This results in a linear interpolation of the phase-specific stiffnesses. In contrast, Schneider et al. [18] presented a scheme which accounts for the mechanical jump conditions

$$\begin{aligned} &[\![\boldsymbol{H}]\!]^{\alpha\beta} = \boldsymbol{a}^{\alpha\beta} \otimes \boldsymbol{n}^{\alpha\beta}, \qquad [\![\boldsymbol{\sigma}]\!]^{\alpha\beta}\, \boldsymbol{n}^{\alpha\beta} = \mathbf{0}, \\ &\text{with } [\![\psi]\!]^{\alpha\beta} = \psi^\alpha - \psi^\beta, \end{aligned} \tag{10}$$

which was recently also applied to single-crack order parameter phase-field models by Prajapati et al. [11] and Hansen-Dörr et al. [12]. Thereby, the first equation resembles a kinematic compatibility, since the deformation gradient $\boldsymbol{H}$ can only exhibit a jump $\boldsymbol{a}^{\alpha\beta}$ in normal direction of the singular surface. In contrast, the balance of linear momentum on a material singular surface, c.f., e.g., Prahs and Böhlke [23], given by eq. (10)b, prohibits a jump of the stress vector normal to the singular surface. Regarding a multiphase-field approach, the normal vector $\boldsymbol{n}^{\alpha\beta}$ of the singular surface between phase α and β and the jump of the infinitesimal strain tensor, regarding the diffuse interface context is given by

$$[\![\boldsymbol{\varepsilon}]\!]^{\alpha\beta} = \mathrm{sym}\left(\boldsymbol{a}^{\alpha\beta} \otimes \boldsymbol{n}^{\alpha\beta}\right), \qquad \boldsymbol{n}^{\alpha\beta} = \frac{\nabla\phi^\alpha - \nabla\phi^\beta}{|\nabla\phi^\alpha - \nabla\phi^\beta|}. \tag{11}$$

In order to solve the governing equations, the unknown jump vectors $\boldsymbol{a}^{\alpha\beta}$ have be to determined. Reformulating the problem as a system of linear equations allows us to determine an effective stiffness for fixed order parameters [12, 18]. Based on a staggered approach, the governing equations are solved iteratively with an additional static criterion for crack propagation [1]. A more detailed introduction to mechanical jump conditions, in the context of a multiphase-field approach, is given by Schneider et al. [18].

4 Results

In this work, a glass fiber reinforced polymer (FRP) is chosen to schematically demonstrate the advantage of considering mechanical jump condition compared to the application of the Voigt-Taylor scheme in the context of MCOP. This material system is motivated by the high contrast regarding the elastic properties of the matrix material, a thermoset, and the glass fiber: A Young's modulus of $E^\mathrm{TS} = 3.45\,\mathrm{GPa}$, and $E^\mathrm{GF} = 73.0\,\mathrm{GPa}$ is assumed for the glass fiber, respectively the thermoset. The Poisson's ratio of fiber and thermoset are $\nu^\mathrm{TS} = 0.38$ and $\nu^\mathrm{GF} = 0.22$ according to [24, 25]. For simplicity, unidirectional reinforced volume elements are used. This allows a reduction to a 2D system. A square with a side length of $100\,\mu\mathrm{m}$ and a volume fraction of $40\,\%$, with a fiber radius of $4\,\mu\mathrm{m}$ is chosen. As boundary conditions, the macroscopic strain tensor

$$\boldsymbol{\varepsilon}(t) = \bar{\varepsilon}_{xx}(t)\, \boldsymbol{e}_x \otimes \boldsymbol{e}_x, \tag{12}$$

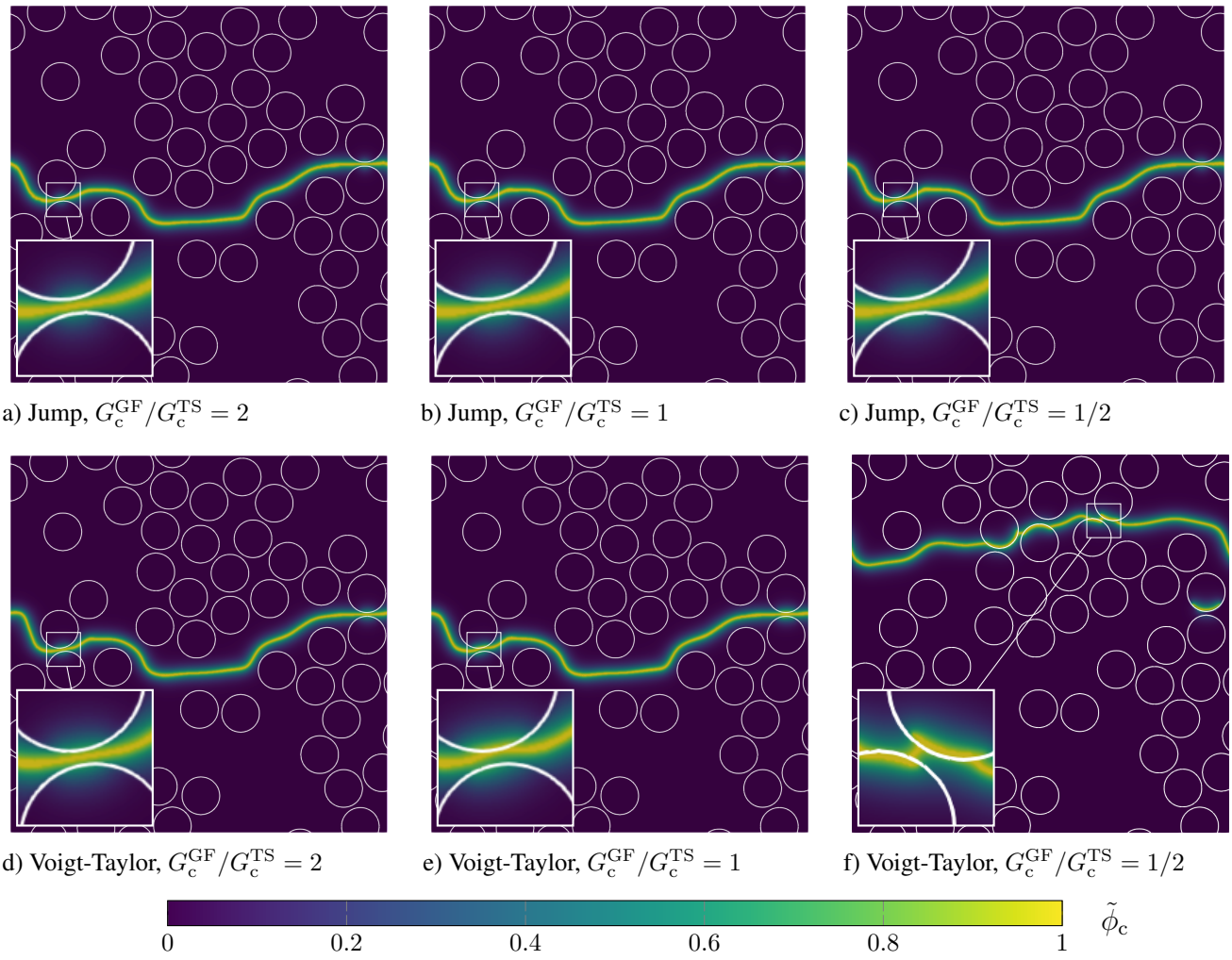

Fig. 3: Crack path of 2D unidirectional fiber reinforced volume elements after failure if jump condition are considered (**a**-**c**) and a Voigt-Taylor scheme (**d**-**f**). In addition, the ratio of the crack resistances G_c^{GF}/G_c^{TS} is varied.

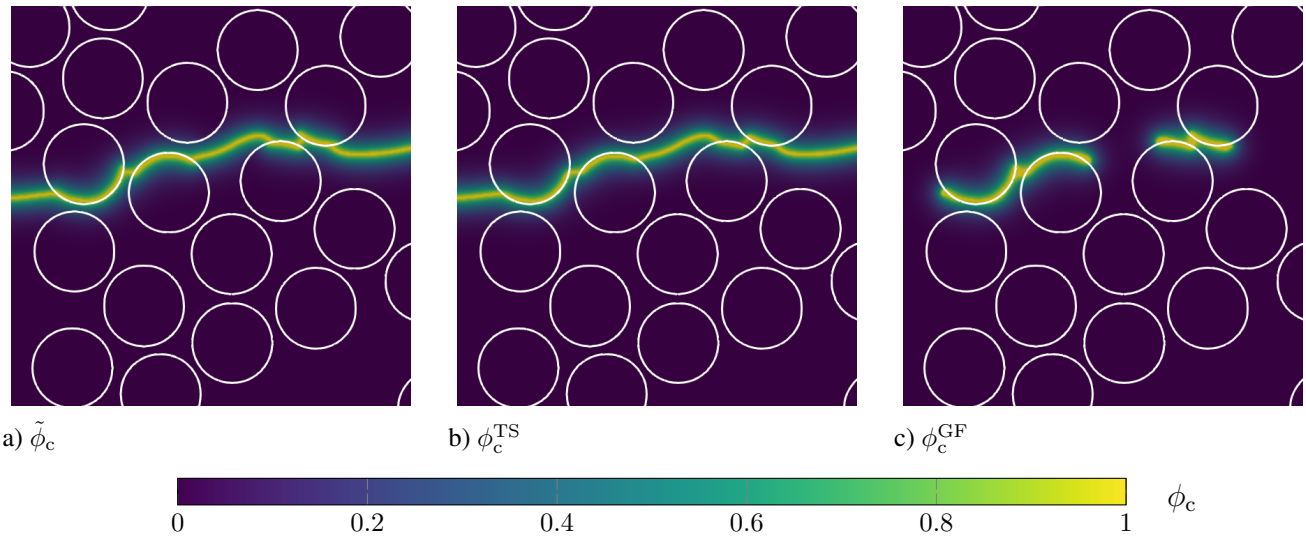

Fig. 4: Detail of the crack path from Figure 3f (Voigt-Taylor, $G_c^{GF}/G_c^{TS} = 1/2$) for the effective crack order parameter $\tilde{\phi}_c$ (**a**), the thermoset crack order parameter ϕ_c^{TS} (**b**), and the glass fiber ϕ_c^{GF} (**c**).

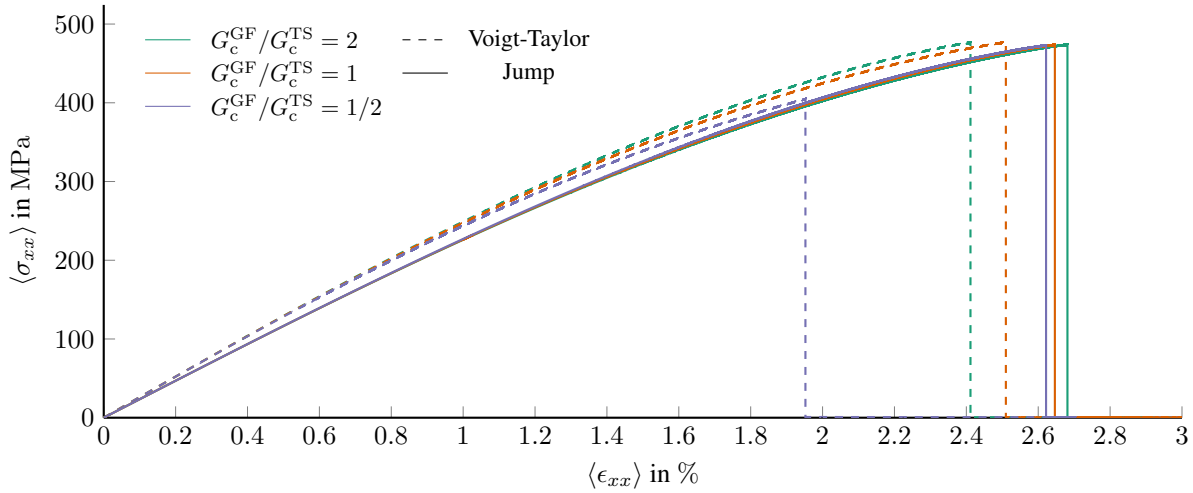

Fig. 5: Macroscopic stress-strain curves of 2D unidirectional fiber reinforced volume elements for a Voigt-Taylor scheme and if jump condition are considered, with $\langle \psi \rangle = \frac{1}{V} \int_\Omega \psi \mathrm{d}v$. In addition, the ratio of the crack resistances G_c^{GF}/G_c^{TS} is varied.

is applied. The function $\bar{\varepsilon}_{xx}(t)$ will be increased linearly with time, until the volume element fails completely. While the crack resistance of the thermoset is kept constant with $G_c^{TS} = 100.0\,\mathrm{J\,m^{-2}}$, the crack resistance of the glass fiber is varied. Despite a failure of the fiber is possible under certain circumstances, a failure of the matrix is expected for all ratios used in this work. With the assumption that the crack surface energy will be minimized and $G_c^{TS} > G_c^{GF}$, failure of the fiber seems preferential. But even for such a case, the matrix can exhibit a lower crack resistance in the sense of stress intensity factors. So not only the crack surface energy, but also the capability to provide this energy, e.g., by a higher Young's modulus, determines which material component fails. In Figure 3 the final crack paths, with the effective crack order parameter field

$$\tilde{\phi}_c = \phi^{TS}\phi_c^{TS} + \phi^{GF}\phi_c^{GF}, \tag{13}$$

are displayed. Regarding the simulations that account for the jump conditions (a-c), the system exhibits the same crack path for all variants. From a nucleation of the crack between close fibers due to stress concentration, a matrix-dominated path is predicted. For the Voigt-Taylor scheme, the two higher ratios (d,e) show the same crack path, even if more fiber damage is present. For the lowest ratio (f) a completely different path is predicted, with damaged fiber, even far away from the final failure crack path. In addition, the crack propagates at the inner side of the fiber interfaces, which is in contrast to the expected behavior. In Figure 4 a detailed section of the Figure 3f is displayed. In addition to the effective crack order parameter field (a), also the crack order parameters fields of the thermoset (b) and glass fiber (b) are provided. In the latter, it can be observed that in addition to the matrix material also the fiber exhibit completely failure, which is in contrast to the expected behavior.

The macroscopic stress-strain curves are displayed in Figure 5. Already in the linear regime of the curves, a difference can be observed: As the Voigt-Taylor scheme describes an upper limit for the elastic energy, it seems reasonable that it exhibits higher stresses. Since it is only accurate for specific cases, such as a parallel material chain, the difference in stress is in accordance to theory [18]. As the failure is dominated by the matrix behavior, the influence of the varied crack resistance of the glass fiber is negligible. However, a small influence during the crack nucleation between two fibers due to the diffuse interface remains. On the contrary, the failures for the Voigt-Taylor scheme occurs at quite different strains. The assumption of same strains for fiber and matrix leads to high driving forces and therefore an earlier failure of fiber and matrix, compared to the case where jump conditions are considered.

5 Conclusion

Schöller et al. [1] proposed a MCOP model for fracture in heterogeneous materials. Despite the improvement in the qualitative and quantitative prediction of crack paths for such systems, the model has some limitations. Therefore, an extension of this model was proposed in this work and investigated: Instead of a basic Voigt-Taylor homogenization scheme, the approach is extended to consider mechanical jump conditions based on Schneider et al. [19]. An exemplary FRP system was introduced to investigate the behavior of both schemes. Therefore, the crack resistance of the glass fiber was varied. The Voigt-Taylor homogenization scheme failed to predict reasonable crack paths for contrary contrasts of elastic modulus and crack resistance. Instead, the fiber failed as well, resulting in different paths. In contrast, when mechanical jump conditions are considered, the model yields the same final crack path for all crack resistances presented, since the mechanical driving force for crack propagation is modeled more independently of the elastic properties of other physical domains. Moreover, this behavior could also observe in the stress-strain curves. While the Voigt-Taylor scheme fails at different loading points, the novel scheme shows a negligible scatter.

Based on this work, more extensive simulation studies on the failure mechanism of FRP materials, as well as other complex systems such as polycrystalline materials, e.g., in hydrothermal environments [26], solid oxide fuel cells among others, can be conducted. Combined with experimentation, this offers the opportunity to improve a broad range of engineering applications. Furthermore, the proposed crack phase field model does not include established extensions such as a tension-compression splitting. In future work, a sophisticated tension-pressure splitting, e.g., [27], could further improve the model. In addition, incorporating plasticity and solid-state phase-field transitions into the model could allow the study of, for example, fracture during martensitic phase transformation [28].

Acknowledgements We thank the German Research Foundation (DFG) for funding main parts of the model development within a partial project of the International Research Training Group IRTG 2078. Furthermore, the authors acknowledge the financial support by the Federal Ministry of Education and Research of Germany in the framework of "ElChFest" (project number 03SF0641A). Support of the Helmholtz program "Material Systems Engineering (MSE)", topic 1 (43.31.01) and the KIT strategy of excellence, future fields project "KaDI4Mat" is gratefully acknowledged. Open access funding enabled and organized by Projekt DEAL.

References

[1] L. Schöller, D. Schneider, C. Herrmann, A. Prahs, and B. Nestler, Computer Methods in Applied Mechanics and Engineering **395**, 114965 (2022).
[2] B. Lawn, Fracture of Brittle Solids (Cambridge University Press, jun 1993).
[3] G. I. Barenblatt, Journal of Applied Mathematics and Mechanics **23**(3), 622–636 (1959).
[4] D. S. Dugdale, Journal of the Mechanics and Physics of Solids **8**(2), 100–104 (1960).
[5] T. P. Fries and T. Belytschko, International Journal for Numerical Methods in Engineering **84**(3), 253–304 (2010).
[6] A. Karma, D. A. Kessler, and H. Levine, Physical Review Letters **87**(4), 45501–1–45501–4 (2001).
[7] B. Bourdin, G. A. Francfort, and J. J. Marigo, Journal of the Mechanics and Physics of Solids **48**(4), 797–826 (2000).
[8] C. Miehe, M. Hofacker, and F. Welschinger, Computer Methods in Applied Mechanics and Engineering **199**(45-48), 2765–2778 (2010).
[9] T. T. Nguyen, J. Réthoré, J. Yvonnet, and M. C. Baietto, Computational Mechanics **60**(2), 289–314 (2017).
[10] D. Schneider, E. Schoof, Y. Huang, M. Selzer, and B. Nestler, Computer Methods in Applied Mechanics and Engineering **312**(dec), 186–195 (2016).
[11] N. Prajapati, C. Herrmann, M. Späth, D. Schneider, M. Selzer, and B. Nestler, Computational Geosciences **24**(3), 1361–1376 (2020).
[12] A. C. Hansen-Dörr, J. Brummund, and M. Kästner, Archive of Applied Mechanics **91**(2), 579–596 (2021).
[13] H. Henry, Theoretical and Applied Fracture Mechanics **104**(dec), 102384 (2019).
[14] A. Durga, P. Wollants, and N. Moelans, Modelling and Simulation in Materials Science and Engineering **21**(5), 55018 (2013).
[15] J. Mosler, O. Shchyglo, and H. Montazer Hojjat, Journal of the Mechanics and Physics of Solids **68**(1), 251–266 (2014).
[16] K. Ammar, B. Appolaire, G. Cailletaud, and S. Forest, European Journal of Computational Mechanics **18**(5-6), 485–523 (2009).
[17] B. Svendsen, P. Shanthraj, and D. Raabe, Journal of the Mechanics and Physics of Solids **112**(mar), 619–636 (2018).
[18] D. Schneider, F. Schwab, E. Schoof, A. Reiter, C. Herrmann, M. Selzer, T. Böhlke, and B. Nestler, Computational Mechanics **60**(2), 203–217 (2017).
[19] D. Schneider, E. Schoof, O. Tschukin, A. Reiter, C. Herrmann, F. Schwab, M. Selzer, and B. Nestler, Computational Mechanics **61**(3), 277–295 (2018).
[20] B. Nestler, H. Garcke, and B. Stinner, Phys. Rev. E **71**(Apr), 041609 (2005).
[21] F. Ernesti, M. Schneider, and T. Böhlke, Computer Methods in Applied Mechanics and Engineering **363**, 112793 (2020).
[22] C. Kuhn and R. Müller, Engineering Fracture Mechanics **77**(18), 3625–3634 (2010), Computational Mechanics in Fracture and Damage: A Special Issue in Honor of Prof. Gross.
[23] A. Prahs and T. Böhlke, Continuum Mechanics and Thermodynamics **32**, 1417–1434 (2019).
[24] A. Trauth, Characterisation and modelling of continuous-discontinuous sheet moulding compound composites for structural applications, 2019.
[25] J. Görthofer, N. Meyer, T. D. Pallicity, L. Schöttl, A. Trauth, M. Schemmann, M. Hohberg, P. Pinter, P. Elsner, F. Henning, A. Hrymak, T. Seelig, K. Weidenmann, L. Kärger, and T. Böhlke, Composites Part B: Engineering **169**, 133–147 (2019).
[26] M. Späth, J. L. Urai, and B. Nestler, Geophysical Research Letters **49**(15), e2022GL098643 (2022).
[27] J. Storm, D. Supriatna, and M. Kaliske, International Journal for Numerical Methods in Engineering **121**(5), 779–805 (2020).
[28] E. Schoof, C. Herrmann, N. Streichhan, M. Selzer, D. Schneider, and B. Nestler, Modelling and Simulation in Materials Science and Engineering **27**(2), 025010 (2019).

